ISMRM British & Irish Chapter Annual Meeting 2024

11th - 13th September

Monica Partridge Building
University of Nottingham
United Kingdom

50+ Years of MRI

Programme

ISMRM | British & Irish CHAPTER

University of Nottingham
UK | CHINA | MALAYSIA

Poster Abstracts

In order of the power pitches in the program schedule

Published 03/09/2024

Ultra-low field Magnetic Resonance Imaging of the human forearm in the Earth's Magnetic Field of Dublin, Ireland.

Friedrich Wetterling[1,2,3], Conor Conway[1], Shane Hunt[1], Arun Bokde[2], and Anil Kokarem[1]
[1]Electronic and Electrical Engineering, Trinity College Dublin, Dublin, Ireland
[2]Trinity College Institute of Neuroscience (TCIN), Trinity College Dublin, Dublin, Ireland
[3]Trinity Centre for Biomedical Engineering (TCBE), Trinity College Dublin, Dublin, Ireland

Introduction: The aim of this work was to explore the limits and opportunities for ultra-low field Magnetic Resonance Imaging in the earth's magnetic field at 50μT (EF-MRI) in Dublin, Ireland. MRI normally requires high static magnetic fields (>0.5T) to polarise the hydrogen-1 nuclei in tissue and to maximise the available signal. Callaghan et al. developed EF-MRI for use in antarctica [1] before advancing the technology to commercialisation as an educational systems globally [2]. Nowadays those systems can be developed at low material cost of less than 200EUR [3, 4]. However, their use has not evolved much beyond scientific and educational exploration. Some universities reported student laboratories for undergraduates using the system in physics [5] and in chemistry [6]. Yet, other examples demonstrated the remaining signal challenges to work with this approach in practice [7].

Fig. 1. *the top image shows the location of the Medical Circuits and Systems laboratory (www.MediCAS-Lab.eu) hosted at the Electronics and Electrical engineering Department at Trinity College Dublin (TCD) in the city centre of Dublin, Ireland. The bottom picture shows the Magritek Earth's Field MRI system positioned for measurements of the forearm.*

Methods: All EF-MRI experiments were carried out on a system with an inner diameter of 80mm (Terranova, Magritek, Wellington, New Zealand, Figure 1) which provided approximately 21mT polarization magnetic field strength using 7A polarization current. The maximum gradient strength was 80μT/m. First-order shimming was achieved by supplying the three-axis gradient coil set with currents of up to 30mA. An autoshim algorithm was applied, employing a modified bisection approach to iterate towards the ideal shim by maximizing the peak height. The B_1-coil was tuned by 9.5nF to 2095Hz Larmor frequency. The Free Induction Decays (FIDs) (Tpol/TB1/Tdelay/Tacq/TR=1.5s/0.65ms/17ms/0.5s/3s, 8192 points) were processed offline using a routine written in MATLAB (Mathworks, Nattick, USA). *EF-MRI* of phantoms filled with tab water were conducted using a 2D filtered back projection sequence (Tpol/TB1/Tdelay/TE/TR=4s/0.7ms/17ms/100ms/8s, 32 projections, 64Hz bandwidth, and 64 samples, for 200x200mm FOV in z-direction and y-direction resulting in a nominal voxel resolution of 3mm x 3mm). The total imaging time was 4min16s. For the forearm the following parameters were reduced: TE to 50ms, Tpol to 1s, TR to 2s, TB1 to 0.66ms, and projections to 16 with 32 samples per projection. The total acquisition time was 32 seconds. Ten FIDs were collected for the forearm (Tpol/TB1/Tdelay/Tacq/TR=1.5s/0.6ms/17ms/0.5s/3s, 8192 points).

Results: Figure 2 shows the raw data captured for a single FID of the water bottle, the filtered result, and the full spectral extend of this signal showing substantial amount of 50-Hz related noise peaks. The resonance was conveniently positioned between the 2150Hz and 2250Hz harmonic noise peaks. Notably, the noise was substantially reduced from ~50μV to ~10μV root mean square through orienting the device 90degree rotated compared to the recommended position – requiring a slight tilt of the system itself. Figure 3 shows the FIDs for 100 recordings within 10 minutes. Expectedly, the noise peak was more stable at a mean and standard deviation of 2151.5±1.0Hz than the water resonance that showed larger variance at 2193.6±3.4Hz translating to a magnetic field strength of 51.52±0.08μT. Figure 4 shows images captured of the water bottle and structured water phantom. Figure 5 shows a spectrum captured of the human forearm and a corresponding first image. While some signal is visible compared to the noise image more work remains to be conducted to substantiate this method.

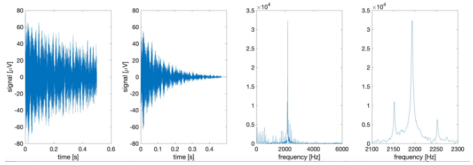

Fig. 2. Free Induction Decay (FID) recorded for a bottle filled with tab water (0.5l). The raw data recorded as a function of time is shown in the graph on the left. The filtered data using an exponential decay time constant at 150ms and 8 times zero filling is shown on the left central graph. The spectrum for that signal is shown in the right central graph demonstrating several harmonic peaks originating from 50 Hz noise. The right graph shows zoomed in spectrum to magnetic resonance of water at 51.4uT (2190Hz).

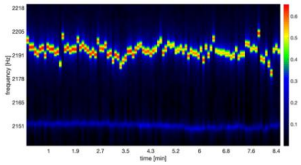

Fig. 3. 100 FIDs captured for water bottle and plotted as a function of time to explore the local magnetic field fluctuations. The mean and standard deviation of the resonance frequency was at 2193.6Hz±3.4 Hz while the 50Hz harmonic at 2150Hz was estimated to be 2151.5±1.0Hz.

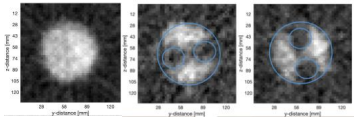

Fig. 4. cross-sectional image of water bottle with 75mm diameter captured using back-projection recording and resonance frequency correction (left). Images from phantom containing two air filled tubes horizontally (centre) and vertically arranged (right).

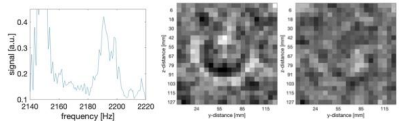

Fig. 5. Magnetic Resonance signal obtained from 10 FIDs for lower arm showing a resonance between 2180 and 2205Hz. Note harmonic of 50Hz at 2150Hz at a much higher magnitude (top). Magnetic Resonance Images obtained Image obtained for lower arm inside scanner (bottom, left) and corresponding noise image when the arm was removed (bottom, right).

Discussion: Imaging of water filled phantoms is easily achievable even in the city centre of Dublin, a major capital city in Europe. However, imaging of tissue remains challenging. The shortened relaxation times in tissue require adaptation of existing solutions. Future systems may facilitate shorter acquisition delays and faster repetition times. Currently, 20ms delay are required before the transmit coil ringdown is complete and before signal can be received and TRs must be twice the polarisation time to prevent overheating of the system. Cooling and more appropriate transmit-only receive-only resonator solutions may offer first innovation approaches to advance EF-MRI further. Sodium-23 MRI suffers from a comparable signal loss as EF-MRI achieving approximately 20 000 less signal than hydrogen-1 MRI, yet while whole body sodium MRI has been captured in 2012 [8], EF-MRI remains to be challenging. The use of SQUIDs and higher pre-polarisation may offer a viable avenue to boost signal for EF-MRI.

Conclusions: In conclusion, EF-MRI offers sufficient signal for MRI of water phantoms. Device positioning and calibration remains challenging and magnetic field variations require correction for imaging. Optimized resonator coils and sequences may offer a new avenue for EF-MRI in the future.

References

[1] P. T. Callaghan, C. D. Eccles, and J. D. Seymour, *Review of Scientific Instruments,* vol. 68, no. 11, pp. 4263-4270, 1997.

[2] M. E. Halse, A. Coy, R. Dykstra, C. Eccles, M. Hunter, R. Ward, and P. T. Callaghan, *J Magn Reson,* vol. 182, no. 1, pp. 75-83, Sep, 2006.

[3] C. A. Michal, *Measurement Science and Technology,* vol. 21, no. 10, pp. 105902, 2010/08/09, 2010.

[4] C. A. Michal, *Journal of Magnetic Resonance,* vol. 319, pp. 106800, 2020/10/01/, 2020.

[5] B. Kami Pars, D. Baudouin, L. Ryma, P.-Q. Marie, and D. Luc, *European Journal of Physics,* vol. 36, no. 3, pp. 035032, apr, 2015.

[6] P. Bergstrom Mann, S. Clark, S. T. Cahill, C. D. Campbell, M. T. Harris, S. Hibble, T. To, A. Worrall, and M. Stewart, *Journal of Chemical Education,* vol. 96, no. 10, pp. 2326-2332, 2019/10/08, 2019.

[7] L. Deshmukh, K. Bagree, and S. Sharma, *International Journal of Engineering Research and Applications,* vol. 07, pp. 26-30, 05/01, 2017.

[8] F. Wetterling, D. M. Corteville, R. Kalayciyan, A. Rennings, S. Konstandin, A. M. Nagel, H. Stark, and L. R. Schad, *Phys Med Biol,* vol. 57, no. 14, pp. 4555-67, Jul 21, 2012.

Tuneable Digital Phantoms for Grey Matter Modelling

1 Cardiff University Brain Research Imaging Centre (CUBRIC), School of Psychology, Cardiff University, Cardiff, United Kingdom. 2 School of Computer Science and Informatics, Cardiff University, Cardiff, United Kingdom. 3 École polytechnique fédérale de Lausanne, Lausanne, Switzerland. 4 Frankfurt Institute for Advanced Studies, Frankfurt am Main, Germany. 5 Ernst Stru¨ngmann Institute (ESI) for Neuroscience in cooperation with the Max Planck Society, Frankfurt am Main, Germany

Introduction: Numerical phantoms play an indispensable role in advancing and validating magnetic resonance imaging (MRI) techniques[1]. This is particularly true of diffusion MRI (dMRI), where the need arises for generating adjustable and microstructurally accurate representations of complex biological tissues. While considerable effort has been dedicated to developing numerical phantoms for brain white matter (WM)[2-4], the same tuneable phantoms capable of replicating the complexity of grey matter (GM) microstructure are lacking. In this work, we introduce *Contextual Cellular Growth* (ConCeG) as a solution to synthesize morphologically accurate GM tissue substrates, employing principles similar to the Contextual Fibre Growth (ConFiG) approach applied to WM[2].

Methods: To create realistic GM phantoms, it is essential to define the key morphological features required to faithfully replicate neural cells, including neurons and glia[5]. We categorized these attributes into three groups: structural, topological, and shape (Fig.1). Real neural cell reconstructions from open-access datasets such as neuromorpho.org[6] and the Allen brain atlas[7] were used to estimate distributions of these morphological features within the GM of the healthy adult mouse brain, utilising the TREES toolbox in MATLAB[8].

ConCeG is the algorithm introduced to synthesize realistic GM phantoms and it is implemented in Matlab. It takes as inputs: voxel size, the number of nodes, predefined morphological parameters (structural, topological, and shape, see Fig.1), and layer-specific density profiles for each cell type. The output consists of cells formatted in SWC[9] format. Similar to ConFiG[2], ConCeG relies on a network of connected nodes. The algorithm starts by distributing soma nodes within specified dimensions, following the user-defined cell density with respect to cortical depth. Additional nodes are randomly placed within the voxel space, creating a connected network for cellular projections. This network serves as a guide for cellular projections to navigate, considering biologically informed cost functions. The projections extend toward attractor points efficiently while avoiding nodes already occupied by existing projections or nodes that would lead to unrealistic projection shrinkage. ConCeG facilitates branching by employing the topological neuron synthesis approach[10]. As a projection grows, its path length increases, and the probability of branching is determined in relation to the birth lengths of remaining bars in the barcode. The branching probability increases as the path length approaches the birth length of another bar and satisfy the probability of branching given the current branch order. Newly initiated branches select angles from the angle distribution and pick attractor points that satisfies this angle in relation to the parent branch. Cellular growth occurs contextually, with the maximum node radius for nodes in the network updated at each growth step.

Results: Fig.2 demonstrates that ConCeG can recreate cellular structures accurately when cells are grown individually, preserving key morphological characteristics' distributions. Fig.3 shows that the same degree of accuracy can be achieved when cells are grown contextually.

Finally, in Fig.4 we illustrate ConCeG's flexibility and capabilities by synthesizing a column of the mouse visual cortex based on density profiles from the Allen brain atlas [11] and [12].

Discussion: Here, we have developed a highly versatile approach, ConCeG, which leverages real cellular data to create realistic digital phantoms of brain GM. These phantoms are ready to be incorporated into dMRI simulators, such as Camino[13], DiSimPy[14] and MCDS[15].

The current implementation of ConCeG enables the generation of large voxels within reasonable computational time (e.g. ~5 hours to generate a 100x100x1200 μm^3 voxel using a single CPU-thread). However, further developments are necessary to achieve dense cellular packing. In fact, the densest voxel we were able to generate thus far has a 54% intracellular volume fraction. Future work will focus on increasing ConCeG ability to achieve denser cellular packings (e.g. ~70%), implementing strategies such as post-growth optimization similar to ConFiG[2]and MEDUSA[4].